Supporting Information

Enhanced ROS generation in AIE-active iridium(III) photosensitizers by cationization engineering for advanced photodynamic therapy

Shanshan Huang, ‡[a] Yuancheng Li, ‡[b] Xiaohan Xie, [b] Jialin Tong, [a] Guo-Gang Shan,*[a] Chao Qin,*[a] Xiyan Xiao,*[c] Qianruo Wang,*[b] Yuanyuan Li[b] and Hualei Wang [b]

[a] *National & Local United Engineering Laboratory for Power Batteries, Department of Chemistry, Northeast Normal University, Changchun 130024, China*

[b] *Key Laboratory of Zoonosis Research, Ministry of Education, College of Veterinary Medicine, Jilin University, Changchun 130062, China*

[c] *Department of Otolaryngology, Shanghai Children's Medical Center, School of Medicine, Shanghai Jiao Tong University, Shanghai 200025, China.*

[*] Corresponding authors.

E-mail address: shangg187@nenu.edu.cn (G-G. Shan), qinc703@nenu.edu.cn (C. Qin), xiaoxy1220@163.com (X. Xiao), wangqianruo@jlu.edu.cn (Q. Wang).

[#] Shanshan Huang and Yuancheng Li contributed equally to this work.

Table of Contents

1. **Materials and characterization techniques**
2. **Scheme S1.** Synthetic routes of the complexes. (i) CH_2Cl_2, methanol, refluxed, 12 h; (ii) acetonitrile, CH_3I, NH_4PF_6, refluxed, 12 h; (iii) ethylene glycol, NH_4PF_6, 150 °C, 24 h.
3. **Fig. S1.** ^{1}H NMR spectrum of **PPI-C0** in DMSO-d_6.
4. **Fig. S2.** ^{13}C NMR spectrum of **PPI-C0** in DMSO-d_6.
5. **Fig. S3** ^{1}H NMR spectrum of **PPI-C1** in DMSO-d_6.
6. **Fig. S4** ^{19}F NMR spectrum of **PPI-C1** in DMSO-d_6.
7. **Fig. S5** ^{13}C NMR spectrum of **PPI-C1** in DMSO-d_6.
8. **Fig. S6** ^{1}H NMR spectrum of **PPI-C2** in DMSO-d_6.
9. **Fig. S7** ^{19}F NMR spectrum of **PPI-C2** in DMSO-d_6.
10. **Fig. S8** ^{13}C NMR spectrum of **PPI-C2** in DMSO-d_6.
11. **Fig. S9** MicrOTOF spectrum of **PPI-C0**
12. **Fig. S10** MicrOTOF spectrum of **PPI-C1**
13. **Fig. S11** MALDI-TOF-MS of **PPI-C2**.
14. **Fig. S12** PL spectra of (A) **PPI-C0** and (B) **PPI-C1** in THF/H_2O mixtures with different water fractions. Concentration: 5×10^{-5} M.
15. **Fig. S13** PL spectra of DCFH-DA in the presence of (A) PBS, (B) **PPI-C0**, (C) **PPI-C1**, and (D) **PPI-C2** Concentration: complexes (2 μM), DCFH-DA (5 μM).
16. **Fig. S14** Absorption spectra of ABDA in the presence of (A) PBS, (B) **PPI-C0**, (C) **PPI-C1**, and (D) **PPI-C2** under white-light (400-700 nm, 100 mW cm^{-2}) irradiation. Concentration: complexes (2 μM), ABDA (20 μM).
17. **Fig. S15** PL spectra of HPF in the presence of (A) PBS, (B) **PPI-C0**, (C) **PPI-C1**, and (D) **PPI-C2** under white-light (400-700 nm, 100 mW cm^{-2}) irradiation. Concentration: complexes (2 μM), HPF (5 μM).
18. **Fig. S16.** PL spectra of DHR123 in the presence of (A) PBS, (B) **PPI-C0**, (C) **PPI-C1**, and (D) **PPI-C2** under white-light (400-700 nm, 100 mW cm^{-2}) irradiation. (E)

Normalized PL intensity of DHR123 in the presence of **PPI-C0**, **PPI-C1** and **PPI-C2** with or without Vc under white-light (400-700 nm, 100 mW cm^{-2}) irradiation. Concentration: complexes (2 μM), DHR123 (5 μM).

19. **Fig. S17** (A) Size distribution of **PPI-C0** NPs, **PPI-C1** NPs, and **PPI-C2** NPs; (B) Stability and PDI changes of **PPI-C0** NPs, **PPI-C1** NPs, and **PPI-C2** NPs during 30 days, inset: TEM images of NPs. Scale bar = 200 μm. (C) PL intensity of **PPI-C0** NPs, **PPI-C1** NPs, and **PPI-C2** NPs in aqueous solution.
20. **Fig. S18** PL spectra of (A) **PPI-C1** NPs and (B) **PPI-C2** NPs in different concentrations.
21. **Fig. S19** PL spectra of DCFH-DA in the presence of (A) PBS, (B) **PPI-C0** NPs, (C) **PPI-C1** NPs, and (D) **PPI-C2** NPs. (E) Time-course plot of DCFH PL intensity enhancement in the presence of **PPI-C0**, **PPI-C1** and **PPI-C2**, respectively, under white-light (400-700 nm, 100 mW cm^{-2}) irradiation. Concentration: NPs (20 μg/mL), DCFH-DA (5 μM).
22. **Fig. S20** Absorption spectra of ABDA in the presence of (A) PBS, (B) **PPI-C0** NPs, (C) **PPI-C1** NPs, and (D) **PPI-C2** NPs. (E) Time-course plot of ABDA decomposition in the presence of **PPI-C0**, **PPI-C1** and **PPI-C2**, respectively, under white-light (400-700 nm, 100 mW cm^{-2}) irradiation. Concentration: NPs (20 μg/mL), ABDA (20 μM).
23. **Fig. S21** PL spectra of HPF in the presence of (A) PBS, (B) **PPI-C0** NPs, (C) **PPI-C1** NPs, and (D) **PPI-C2** NPs. (E) Time-course plot of HPF PL intensity enhancement in the presence of **PPI-C0**, **PPI-C1** and **PPI-C2**, respectively, under white-light (400-700 nm, 100 mW cm^{-2}) irradiation. Concentration: NPs (20 μg/mL), HPF (5 μM).
24. **Fig. S22** PL spectra of DHR123 in the presence of (A) PBS, (B) **PPI-C0** NPs, (C) **PPI-C1** NPs, and (D) **PPI-C2** NPs. (E) Normalized PL intensity of DHR123 in the presence of **PPI-C0**, **PPI-C1** and **PPI-C2** NPs with or without Vc. (F) Time-course plot of DHR123 PL intensity enhancement of in the presence of **PPI-C0**, **PPI-C1** and **PPI-C2**, respectively, under white-light (400-700 nm, 100 mW cm^{-2}) irradiation. Concentration: NPs (20 μg/mL), DHR123 (5 μM).

25. **Fig. S23** Viability of Hela cells incubated with (A) **PPI-C0** and (B) **PPI-C1** NPs at different concentrations upon white-light (400-700 nm, 100 mW cm^{-2}) irradiation for 15 min.
26. **Fig. S24** Live/dead cell staining assays using FDA and PI as indicators treated with **PPI-C0** or **PPI-C1** NPs upon white light (400-700 nm, 100 mW cm^{-2}) irradiation for 15 min. Scale bar = 40 μm.
27. **Fig. S25** Apoptosis analysis of Hela cells after different treatments with various formulations by FACS.
28. **Fig. S26** CLSM images of HeLa cells incubated with (A) **PPI-C0** or (B) **PPI-C1** NPs for 8 h, followed by costaining with Lyso-tracker green or Mito-tracker green for 5 or 30 min. Scale bar = 20 μm. Concentration: NPs (10 μg/mL), Lyso-tracker green (25 nM), Mito-tracker green (100 nM).
29. **Fig. S27** Intracellular ROS generation by **PPI-C0** NPs and **PPI-C1** NPs with white light (400-700 nm, 100 mW cm^{-2}) irradiation inside Hela cells: (A) DCFH-DA for total ROS, (B) SOSG for $^1O_2$, (C) HPF for •OH, and (D) DHE for $•O_2^-$. Scale bar = 40 μm. Concentration: DCFH (10 μM), SOSG (10 μM), DHE (10 μM), HPF (10 μM).
30. **Fig. S28** Intracellular ROS generation by **PPI-C0** NPs, **PPI-C1** NPs and **PPI-C2** NPs without irradiation inside Hela cells: (A) DCFH-DA for total ROS, (B) SOSG for $^1O_2$, (C) HPF for •OH, and (D) DHE for $•O_2^-$. Scale bar = 40 μm. Concentration: DCFH (10 μM), SOSG (10 μM), DHE (10 μM), HPF (10 μM).
31. **Fig. S29** Blood test results for treated BALB/c mice.
32. **Table S1** Calculated excitation energies of the lowest triplet states (T_1) of **PPI-C0, PPI-C1 and PPI-C2**, dominant orbital excitations and oscillator strength.

Materials and characterization techniques

All reagents were commercially available and used as supplied without further purification. The ^{1}H and ^{13}C NMR spectra of all the molecules were performed on a Bruker Avance NMR spectrometer operating at 500 MHz with tetramethylsilane as the internal standard using DMSO-d_6 as the solvent. Photoluminescence (PL) emission spectra of emitters in acetonitrile-ethanol (5.0×10^{-5} M) and **PPI-C0**, **PPI-C1**, and **PPI-C2** NPs (100 μg/mL) were recorded by using a FL-4600 fluorescent spectrophotometer. UV-vis absorption spectra were recorded on a Hitachi UV-3900 spectrophotometer. The size distribution of NPs was determined by Malvern Zetasizer Nano ZSE. The images of cell fluorescence imaging were recorded by Laser scanning confocal microscope (LSCM-FV3000) from Olympus.

Preparation of Ir-NPs

Ir(III) complex (1 mg) and DSPE-PEG_{2000} (2 mg) were first dissolved in 1 mL THF under sonication for 5 min, and then added quickly to distilled water under sonication for another 10 min. The obtained nanoparticles (Ir-NPs) were filtered through 0.45 and 0.22 μm syringe filter, and then purified and collected by ultrafiltration for 8 min at 8000 rpm with a molecular weight of 1 kDa. Finally, the nanoparticles (Ir-NPs) were suspended in distilled water at a concentration of 1 mg/mL and stored at 4 °C for further use.

Detection of total ROS production in aqueous solution

Total ROS production of **PPI-C0**, **PPI-C1**, and **PPI-C2** in aggregate states were investigated by using the ROS indicator DCFH-DA. The pre-activated DCFH-DA solution (40 μM) was added to the sample aqueous solution (2 μM). Then, the mixed solution was irradiated with white light (100 mW cm^{-2}) for 60 s. After each interval of irradiation, the fluorescence of DCFH-DA at 525 nm, which corresponding to ROS production, was measured by fluorescence spectrometer under the excitation of 488 nm light. Total ROS production of **PPI-C0**, **PPI-C1**, and **PPI-C2** NPs (20 μg/mL) were investigated by the same method.

Detection of type I ROS production in aqueous solution

Type I ROS production efficiency of **PPI-C0**, **PPI-C1**, and **PPI-C2** in aggregate states were investigated by using HPF as the indicator of •OH and DHR123 as the indicator of $•O_2^-$. HPF solution (5 mM) was added to the sample aqueous solution (2 μM). Then, the mixed solution was irradiated with white light (100 mW cm^{-2}). After each interval of irradiation, the fluorescence of HPF at 515 nm, which corresponding to type I ROS, was measured by fluorescence spectrometer under the excitation of 490 nm light. The detection of $•O_2^-$ with DHR123 was carried out in the same method as HPF with fluorescence of 525nm, under the excitation of 495 nm light. The production of **PPI-C0**, **PPI-C1**, and **PPI-C2** NPs (20 μg/mL) were investigated by the same method.

Detection of type II ROS production in aqueous solution

Type II ROS production efficiency of **PPI-C0**, **PPI-C1**, and **PPI-C2** in aggregate states were investigated by using 9,10-dimethylanthrancene (ABDA) as the indicator of $^1O_2$. ABDA dissolved with DMSO solution (2 mM) was added to the sample solution (2 μM). Then, the mixed solution was irradiated with white light (100 mW cm^{-2}). After each interval of irradiation, the absorption spectra ranging from 300 to 420 nm was measured by UV–vis spectrophotometer. The production of **PPI-C0**, **PPI-C1**, and **PPI-C2** NPs (20 μg/mL) were investigated by the same method.

Theoretical calculations

The Gaussian 09 program was utilized to perform DFT calculations. The optimized geometries and electron configurations were investigated using the density functional theory (DFT) and time-dependent DFT (TDDFT) at the B3LYP level. The LANL2DZ basis set was used to treat the Ir atom, whereas the 6-31G** basis set was used to treat C, H, O, N atoms. The geometries of the singlet ground state and the lowest-energy triplet states were fully optimized without imposing any symmetry restriction. Solvent effects were considered within the SCRF (self-consistent reaction field) theory using the polarized continuum model (SMD) approach to model the interaction with the solvent (acetonitrile). The geometries of the triplet states were

then calculated at the spin-unrestricted UB3LYP level with a spin multiplicity of 3 based on the optimized S_0 geometries.

Cell culture and cytotoxicity Assay

Hela cells were cultured in DMEM medium that contain 10% FBS at 37 °C in a 5 % CO_2 atmosphere. Hela cells were cultured in 96-well plates at a density of 3×10^4 cells per well for 24 h. Then, the Ir-NPs with different concentrations were added in wells and incubated for another 8 h. The cells were exposed to white irradiation (100 mW cm^{-2}) for 15 min after replacing the medium, and the dark group was conducted without light irradiation. After incubation for another 12 h, 10 μL CCK-8 was added to each well and the absorption at 450 nm for each well was recorded half an hour later using an enzyme marker.

Intracellular ROS production

Hela cells were seeded in a 6-well plate and incubated for 24 h. Then the cells were co-cultured with Ir-NPs (10 μg/mL) for 8 h, respectively. The dishes were washed 3 times with PBS and the ROS indicator DCFH-DA (10 μM) was then added in the dark and incubated for another 20 min. After that, white light (100 mW cm^{-2}) was used to irradiate the cells for 1 min. Finally, the dishes were imaged by CLSM. The 488 nm laser was applied for excitation and the filter of 500–550 nm was used for signal collection. The detection of $^1O_2$, •OH and•O_2^- were treated as same as total ROS, with SOSG (10 μM), DHE (10 μM), and HPF (20 μM), respectively.

Live/Dead cell staining assay

Hela cells were seeded in 6-well plate and incubated for 24 h. Then the cells were co-cultured with Ir-NPs for 8 h, respectively. After exposed to white light irradiation (100 mW cm^{-2}) for 15 min, the cells were further incubated for another 24 h. The dishes were washed 3 times with PBS and then further incubated with FDA (2 μg/mL) and PI (2 μg/mL) in DMEM for 20 min. Finally, the dishes were imaged by CLSM. The 488 nm laser was applied for excitation of FDA and the filter of 550–600 nm was used for signal collection; 561 nm laser was applied for excitation of PI and the filter of 550–600 nm was used for signal collection.

Animals and tumor model

Healthy BALB/c nude mice (female, 4–6 weeks) were obtained from Liaoning Changsheng biotechnology. The mice were housed under pathogen-free conditions and fed with standard laboratory water and chow. All procedures were performed under the protocol of the Scientific Ethics Committee of Jilin University (SY202407021). To establish the xenograft 4T1-tumor-bearing mouse models, 4T1 cancer cells (5×10^6) suspended in PBS were injected subcutaneously into the right flanks of each mouse. After 10 days, mice with tumor volumes at about 100 mm^3 were used subsequently. Tumor volume was calculated by the following equation: Volume = ((tumor length) × (tumor width)^2)/2.

In vivo photodynamic therapy

To investigate the in vivo antitumor efficacy of **PPI-C2** NPs, xenograft 4T1-tumor-bearing mice were divided into four groups, including PBS, PBS + L, **PPI-C2** NPs, and **PPI-C2** NPs + L (n = 3). When the tumor volume reached about 100 mm^3, 100 μL of PBS or **PPI-C2** NPs (500 μg/mL) were intratumorally injected into mice. For the PBS+L and **PPI-C2** NPs + L groups, the mice were continuously irradiated with white light (100 mW cm^{-2}) for 30 min after post-injection. By contrast, the PBS and **PPI-C2** NPs groups were treated without irradiation. After 14 days of treatment, all the mice were sacrificed for histological analysis. The tumor size was measured by using a vernier caliper, and the weights of mice were also recorded.

Histological and hematological analyses

All the mice were sacrificed after complete treatment of 14 days. Tumors and the major organs (heart, liver, spleen, lung and kidney) were dissected from the mice. After the tissues were fixed in 4 % (v/v) formalin overnight, they were embedded in paraffin and sectioned at 5 mm thickness. The sections were then subjected to H&E staining for histopathological evaluation. The tissue slices were imaged by an inverted optical microscopy. To investigate the biosafety of treatment, the major organs (heart, liver, spleen, lung, and kidney) of each mouse were also excised, and H&E staining was performed in the same procedures.

Synthesis and Characterization

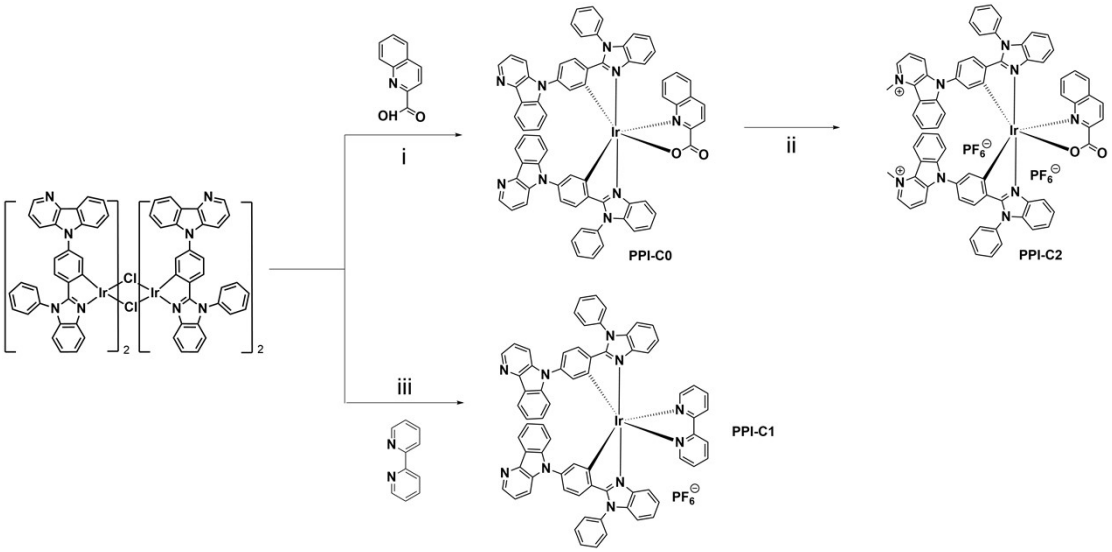

Scheme S1. Synthetic routes of the complexes. (i) CH_2Cl_2, methanol, refluxed, 12 h; (ii) acetonitrile, CH_3I, NH_4PF_6, refluxed, 12 h; (iii) ethylene glycol, NH_4PF_6, 150 °C, 24 h.

Synthesis of PPI-C0. The corresponding μ-chloro-bridged dimer (213 mg, 0.1 mM), the auxiliary ligand quinoline-2-carboxylic acid (37 mg, 0.21 mM) and K_2CO_3 (33 mg, 0.24 mM) were suspended in a mixed solvent of CH_2Cl_2 and ethanol. The mixture was refluxed overnight under an inert atmosphere of nitrogen in darkness. After being cooled to room temperature, the residue was purified by silica gel column chromatography to give **PPI-C0** with orange powder. ^{1}H NMR (500 MHz, DMSO-d_6) δ 8.81 (d, J = 8.5 Hz, 1H), 8.50 – 8.45 (m, 2H), 8.32 (d, J = 8.3 Hz, 1H), 8.27 (d, J = 8.9 Hz, 1H), 8.23 (d, J = 8.2 Hz, 1H), 8.19 (t, J = 7.5 Hz, 2H), 7.91 (dd, J = 11.6, 8.0 Hz, 2H), 7.86 (t, J = 7.2 Hz, 1H), 7.82 – 7.68 (m, 6H), 7.61 (dt, J = 8.7, 4.6 Hz, 1H), 7.55 – 7.49 (m, 2H), 7.43 – 7.40 (m, 2H), 7.37 (t, J = 7.8 Hz, 1H), 7.28 (dd, J = 13.1, 7.3 Hz, 6H), 7.21 – 7.12 (m, 6H), 7.08 (d, J = 8.1 Hz, 1H), 6.99 (d, J = 3.4 Hz, 1H), 6.97 (d, J = 4.1 Hz, 1H), 6.95 (d, J = 6.3 Hz, 1H), 6.91 (dd, J = 8.4, 1.7 Hz, 2H), 6.82 (t, J = 7.7 Hz, 1H), 6.49 (d, J = 2.1 Hz, 1H), 5.72 (d, J = 8.3 Hz, 1H). ^{13}C NMR (126 MHz, DMSO-d_6) δ 174.35, 162.48, 162.27, 154.99, 153.49, 150.27, 147.62, 142.93, 141.85, 141.82, 140.84,

140.61, 140.39, 139.12, 137.61, 137.07, 136.60, 136.38, 134.43, 134.32, 133.59, 133.39, 133.18, 131.60, 131.52, 131.45, 131.34, 131.22, 131.18, 131.14, 130.69, 129.73, 129.65, 129.54, 128.65, 128.50, 128.38, 128.30, 128.12, 127.26, 126.22, 125.11, 124.72, 124.49, 123.93, 122.50, 122.46, 121.42, 121.26, 120.94, 120.80, 119.03, 118.36, 117.31, 117.25, 115.66, 113.70, 112.13, 111.85, 110.50, 110.45.

Synthesis of PPI-C1. The corresponding μ-chloro-bridged dimer (213 mg, 0.1 mM) and the auxiliary ligand 2,2'-bipyridine (33 mg, 0.21 mM) were suspended in ethylene glycol. The mixture was stirred under an inert atmosphere of nitrogen in darkness at 150 °C for 24 h. After being cooled to room temperature, NH_4PF_6 aqueous solution was added and stirred for 2 h. The crude product was obtained by suction filtration and purified by flash column chromatography to give **PPI-C1** with bright yellow powder. ^{1}H NMR (500 MHz, DMSO-d_6) δ 8.98 (d, J = 8.2 Hz, 1H), 8.52 (d, J = 5.5 Hz, 1H), 8.48 – 8.43 (m, 2H), 8.19 (dd, J = 6.1, 3.1 Hz, 1H), 8.01 – 7.96 (m, 1H), 7.81 – 7.76 (m, 3H), 7.67 (t, J = 7.5 Hz, 1H), 7.55 (d, J = 8.3 Hz, 1H), 7.29 (dd, J = 6.2, 3.0 Hz, 2H), 7.23 (dddd, J = 19.9, 12.5, 7.1, 3.9 Hz, 5H), 7.14 (t, J = 7.8 Hz, 1H), 6.97 (dd, J = 12.1, 8.3 Hz, 2H), 6.78 (d, J = 2.1 Hz, 1H), 5.87 (d, J = 8.2 Hz, 1H). ^{19}F NMR (471 MHz, DMSO-d_6) δ -69.38, -70.89. ^{13}C NMR (126 MHz, DMSO-d_6) δ 162.07, 156.88, 154.21, 151.93, 143.09, 141.96, 140.75, 140.31, 138.64, 138.15, 136.61, 134.20, 133.12, 132.77, 131.47, 131.35, 131.21, 130.03, 129.55, 128.71, 128.37, 128.23, 127.22, 125.39, 125.15, 124.96, 122.63, 121.44, 120.94, 120.80, 119.81, 117.57, 113.47, 112.40, 110.66.

Synthesis of PPI-C2. To a stirred solution of **PPI-C0** in acetonitrile under nitrogen atmosphere, iodomethane was added and then heated to reflux overnight. The obtained mixture was evaporated and redissolved in methanol, followed by adding saturated NH_4PF_6 solution. After stirring for 2 h, the crude product was obtained by suction filtration and purified by flash column chromatography to give **PPI-C2** with orange powder. ^{1}H NMR (500 MHz, DMSO-d_6) δ 8.97 – 8.92 (m, 2H), 8.83 (d, J = 8.4 Hz, 1H), 8.59 (d, J = 8.5 Hz, 2H), 8.34 (dd, J = 8.7, 5.4 Hz, 2H), 8.24 (d, J = 8.1 Hz, 1H),

7.96 (d, J = 7.9 Hz, 1H), 7.93 – 7.83 (m, 5H), 7.79 (td, J = 7.3, 6.9, 3.2 Hz, 4H), 7.74 – 7.69 (m, 2H), 7.67 – 7.63 (m, 2H), 7.60 (q, J = 6.4 Hz, 4H), 7.41 (dd, J = 5.7, 3.7 Hz, 1H), 7.32 – 7.25 (m, 3H), 7.20 (d, J = 7.6 Hz, 1H), 7.12 (t, J = 7.8 Hz, 2H), 7.06 (d, J = 8.4 Hz, 2H), 7.02 – 6.94 (m, 4H), 6.89 (d, J = 8.2 Hz, 1H), 6.76 (t, J = 7.8 Hz, 1H), 6.53 (s, 1H), 5.55 (d, J = 8.3 Hz, 1H), 4.82 (d, J = 5.0 Hz, 6H). ^{19}F NMR (471 MHz, DMSO-d_6) δ -69.37, -70.89. ^{13}C NMR (126 MHz, DMSO-d_6) δ 174.54, 161.95, 161.79, 154.76, 153.73, 151.07, 147.43, 142.39, 142.11, 141.13, 139.29, 139.23, 139.16, 138.96, 136.89, 136.77, 136.60, 136.41, 135.36, 135.29, 135.12, 134.84, 134.33, 134.17, 133.33, 132.26, 131.91, 131.60, 131.55, 131.49, 131.27, 131.23, 130.83, 130.67, 129.83, 129.68, 128.69, 128.62, 128.48, 128.34, 127.42, 126.50, 125.20, 124.88, 124.74, 123.90, 123.10, 120.29, 119.56, 115.66, 115.28, 115.23, 113.82, 112.38, 112.06, 46.88.

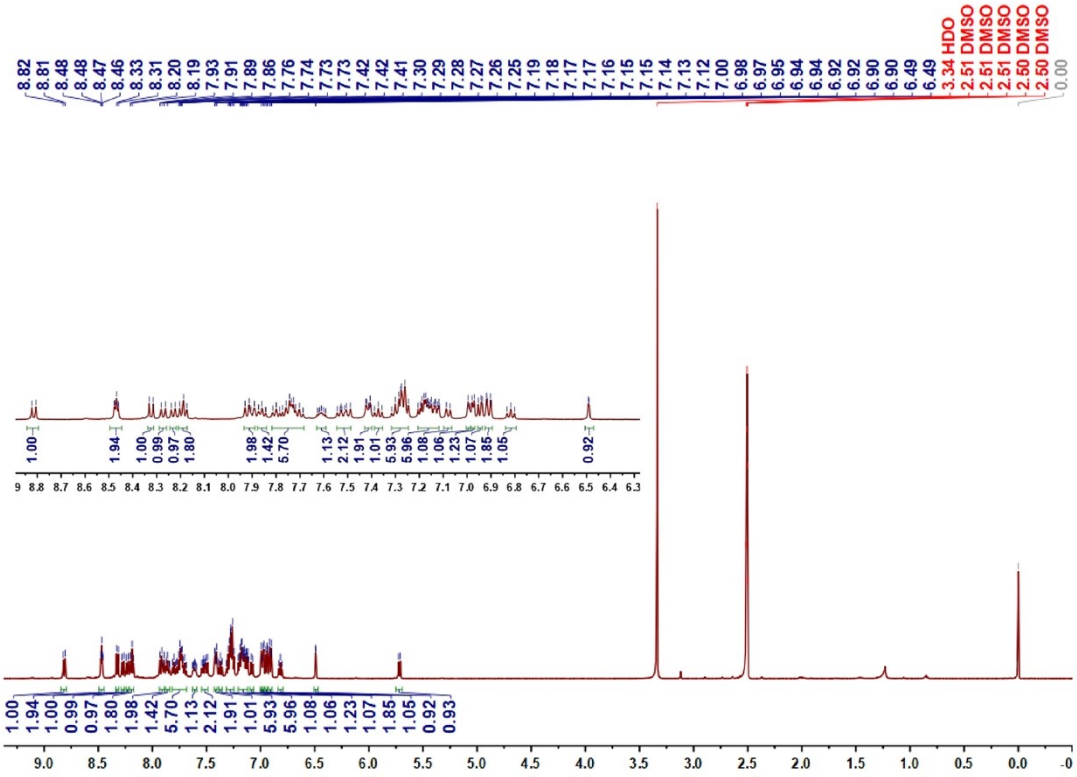

Fig. S1. ^{1}H NMR spectrum of **PPI-C0** in DMSO-d_6.

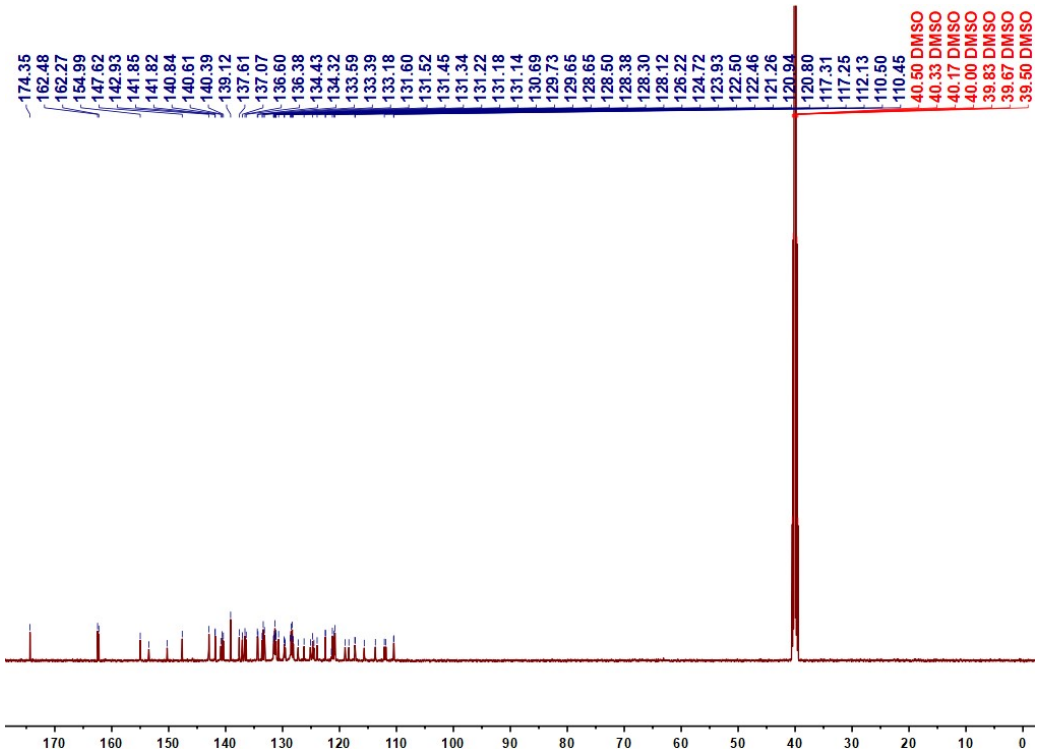

Fig. S2. ^{13}C NMR spectrum of **PPI-C0** in DMSO-d_6.

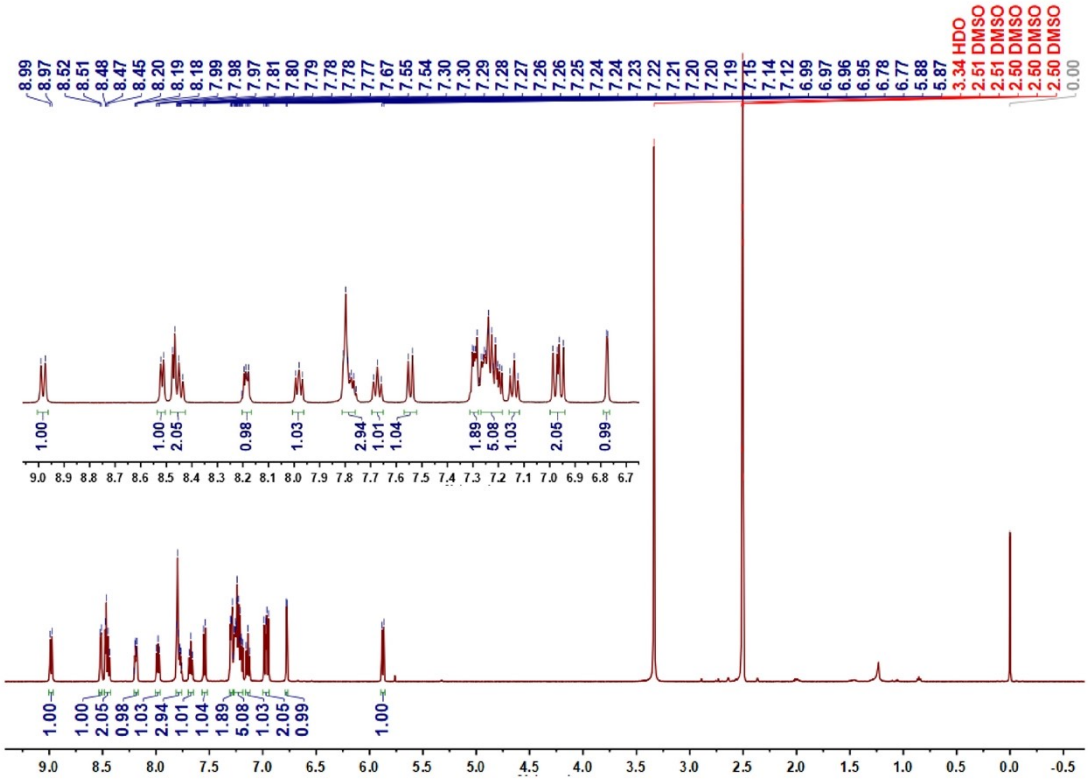

Fig. S3. ^{1}H NMR spectrum of **PPI-C1** in DMSO-d_6.

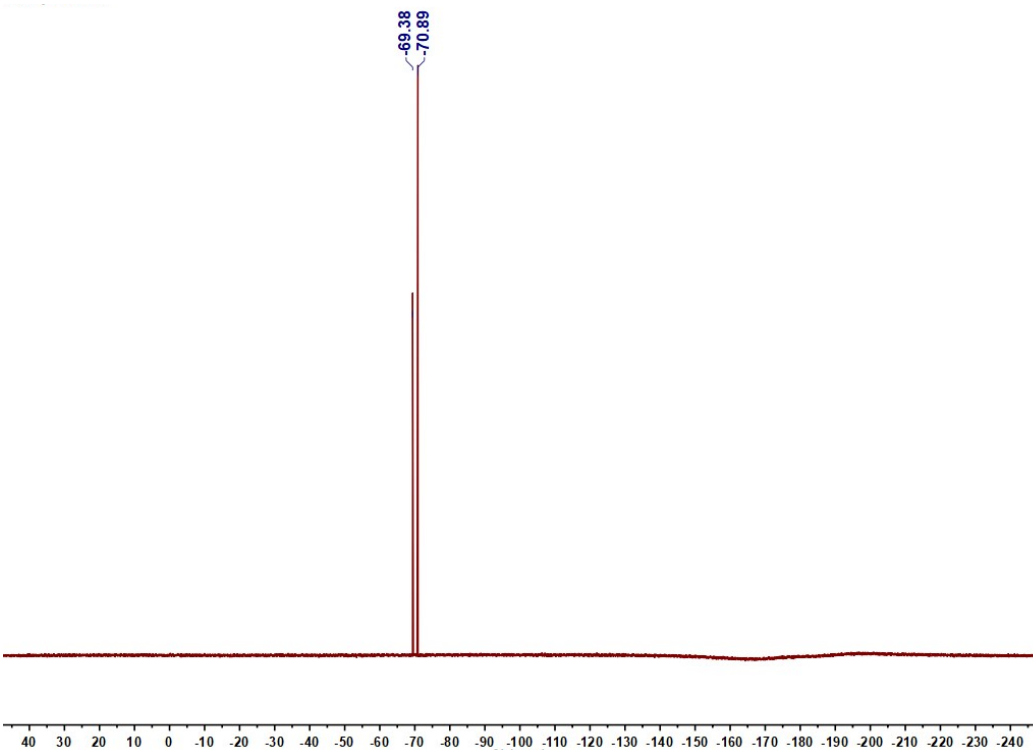

Fig. S4. ^{19}F NMR spectrum of **PPI-C1** in DMSO-d_6.

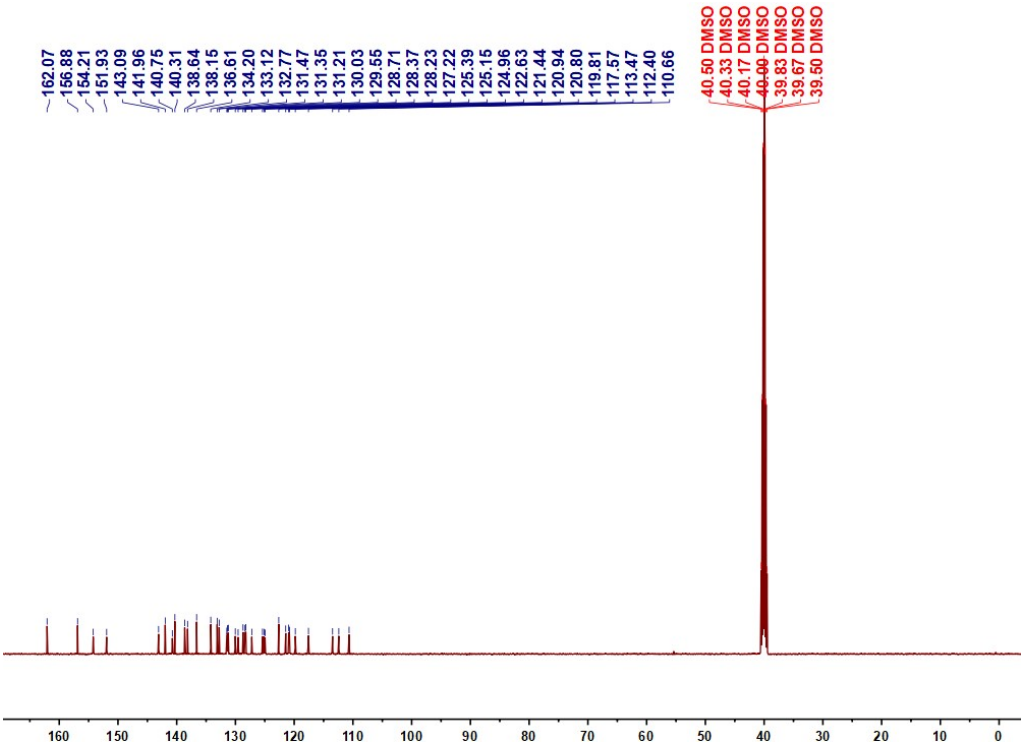

Fig. S5. ^{13}C NMR spectrum of **PPI-C1** in DMSO-d_6.

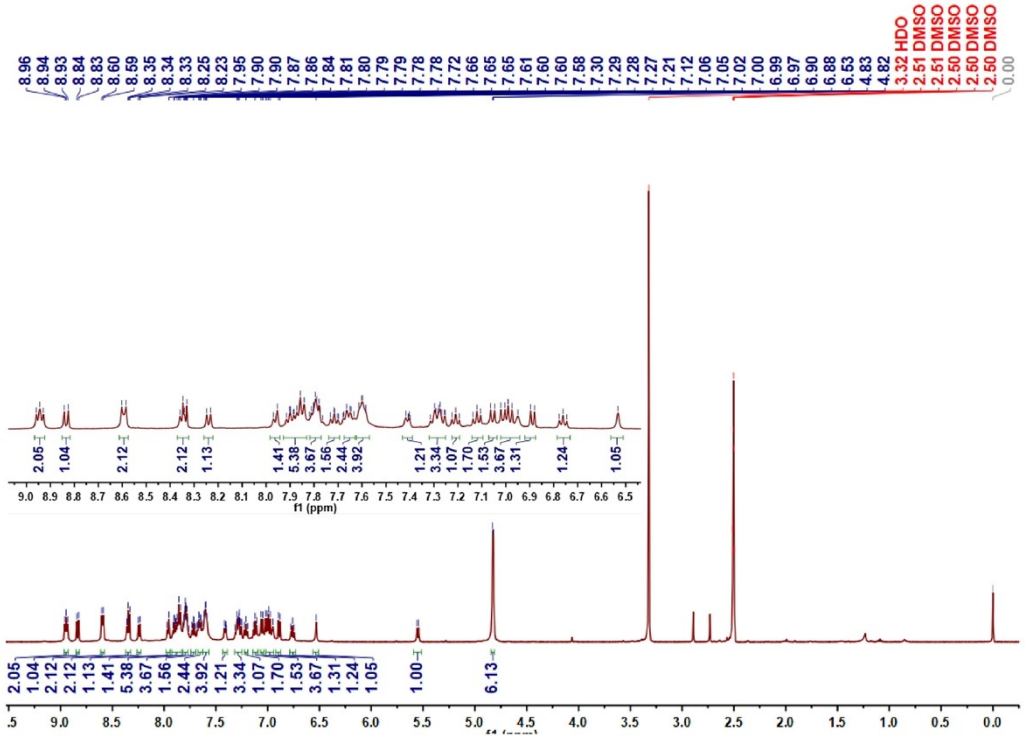

Fig. S6. ^{1}H NMR spectrum of **PPI-C2** in DMSO-d_6.

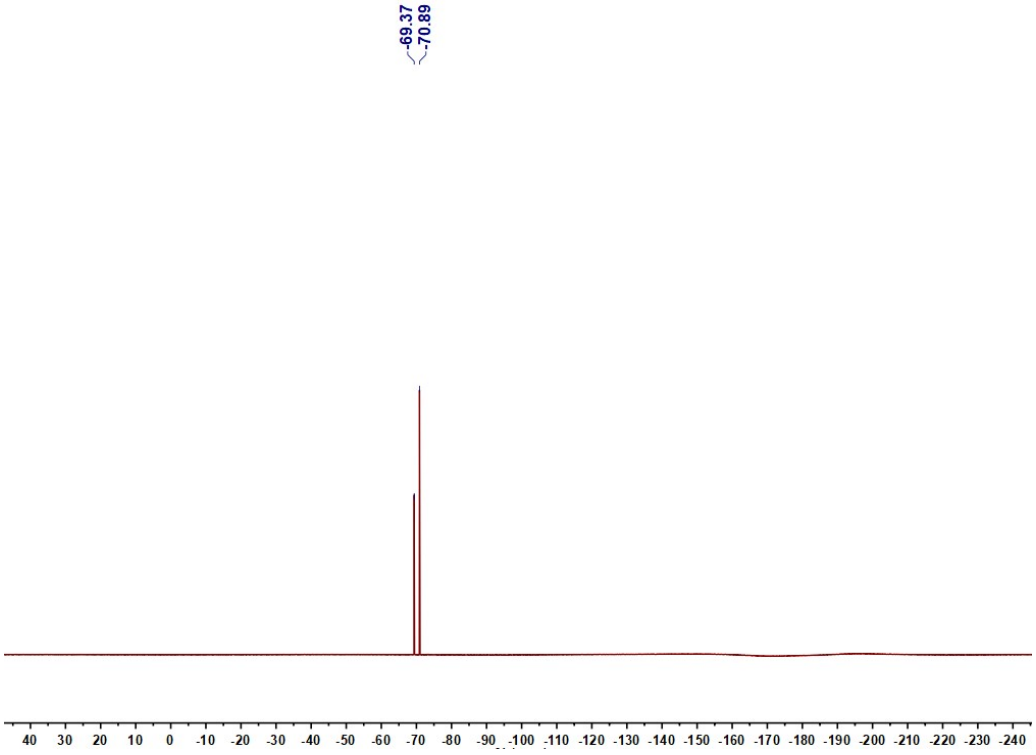

Fig. S7. ^{19}F NMR spectrum of **PPI-C2** in DMSO-d_6.

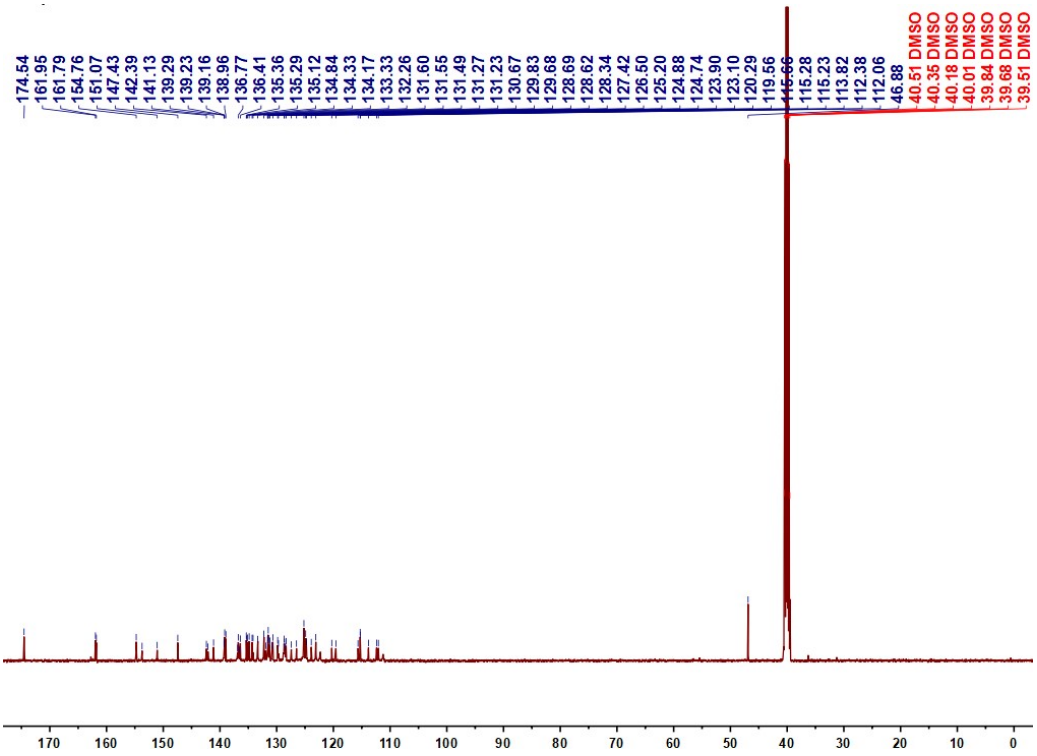

Fig. S8. ^{13}C NMR spectrum of **PPI-C2** in DMSO-d_6.

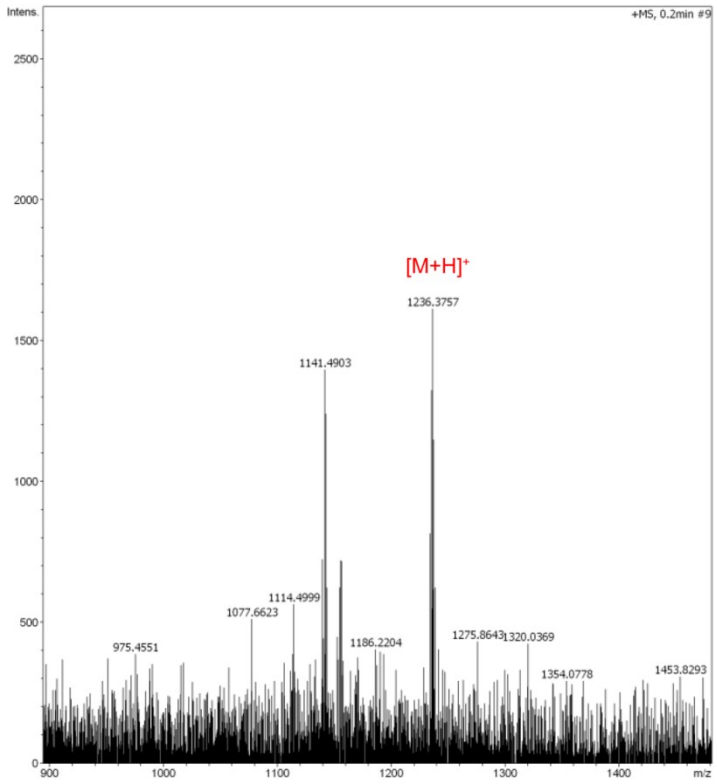

Fig. S9. MicrOTOF spectrum of **PPI-C0**.

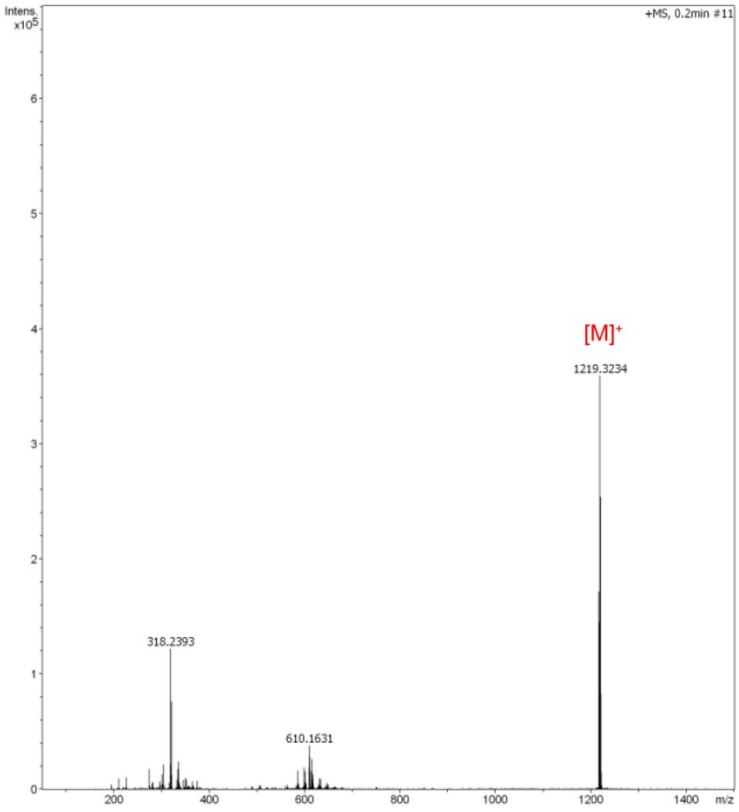

Fig. S10. MicrOTOF spectrum of **PPI-C1**.

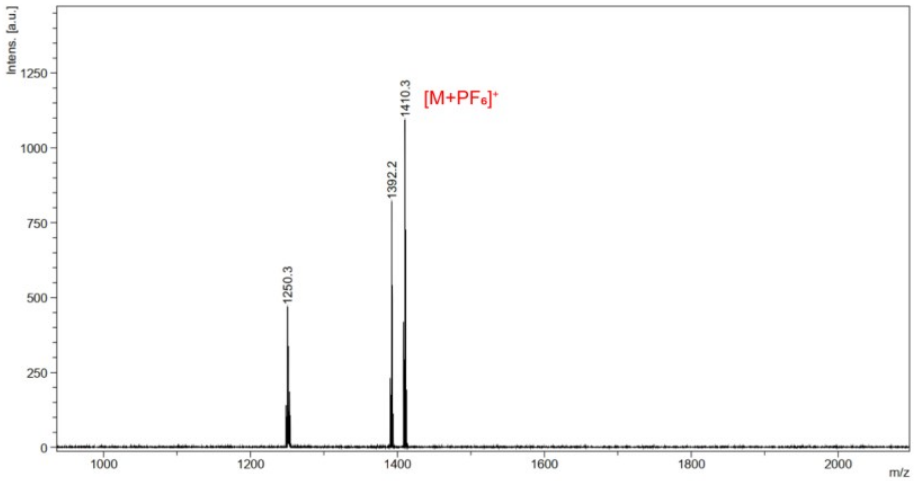

Fig. S11. MALDI-TOF-MS of **PPI-C2**.

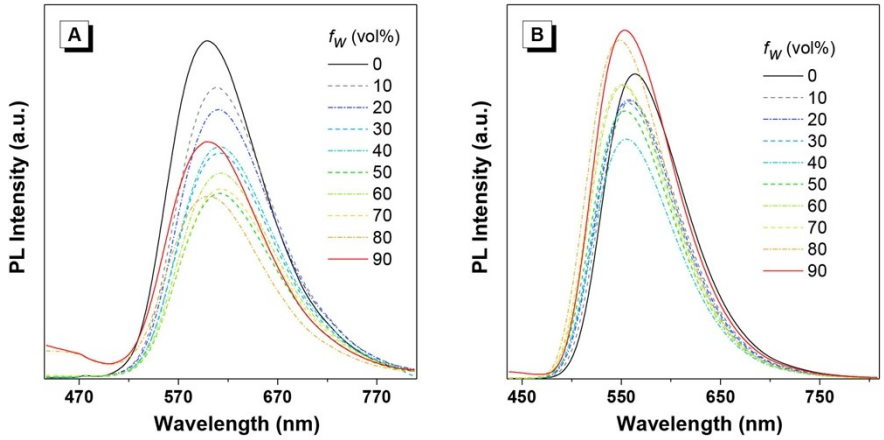

Fig. S12. PL spectra of (A) **PPI-C0** and (B) **PPI-C1** in THF/H_2O mixtures with different water fractions. Concentration: 5×10^{-5} M.

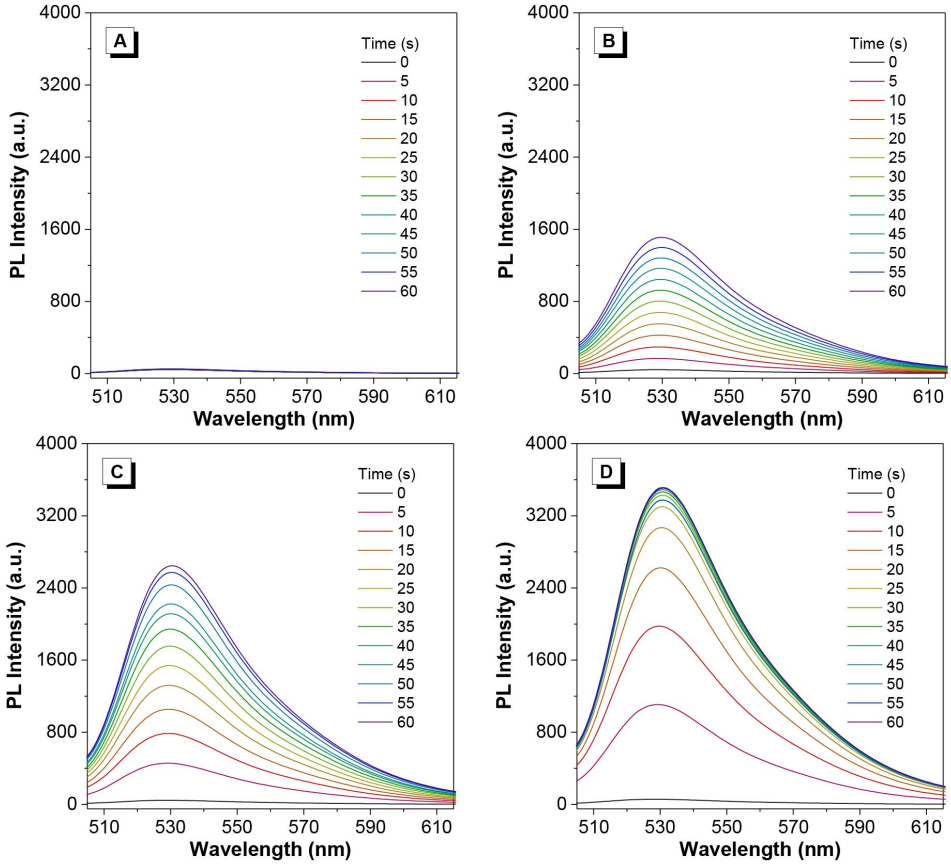

Fig. S13. PL spectra of DCFH-DA in the presence of (A) PBS, (B) **PPI-C0**, (C) **PPI-C1**, and (D) **PPI-C2** under white-light (400-700 nm, 100 mW cm^{-2}) irradiation. Concentration: complexes (2 μM), DCFH-DA (5 μM).

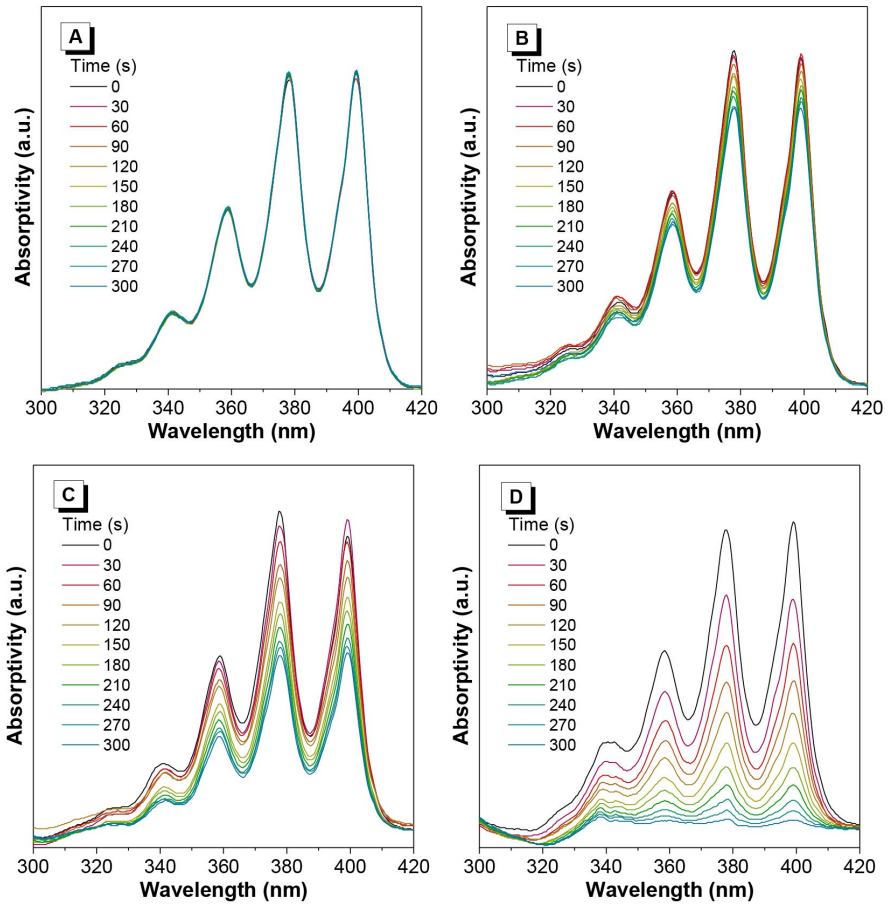

Fig. S14. Absorption spectra of ABDA in the presence of (A) PBS, (B) **PPI-C0**, (C) **PPI-C1**, and (D) **PPI-C2** under white-light (400-700 nm, 100 mW cm^{-2}) irradiation. Concentration: complexes (2 μM), ABDA (20 μM).

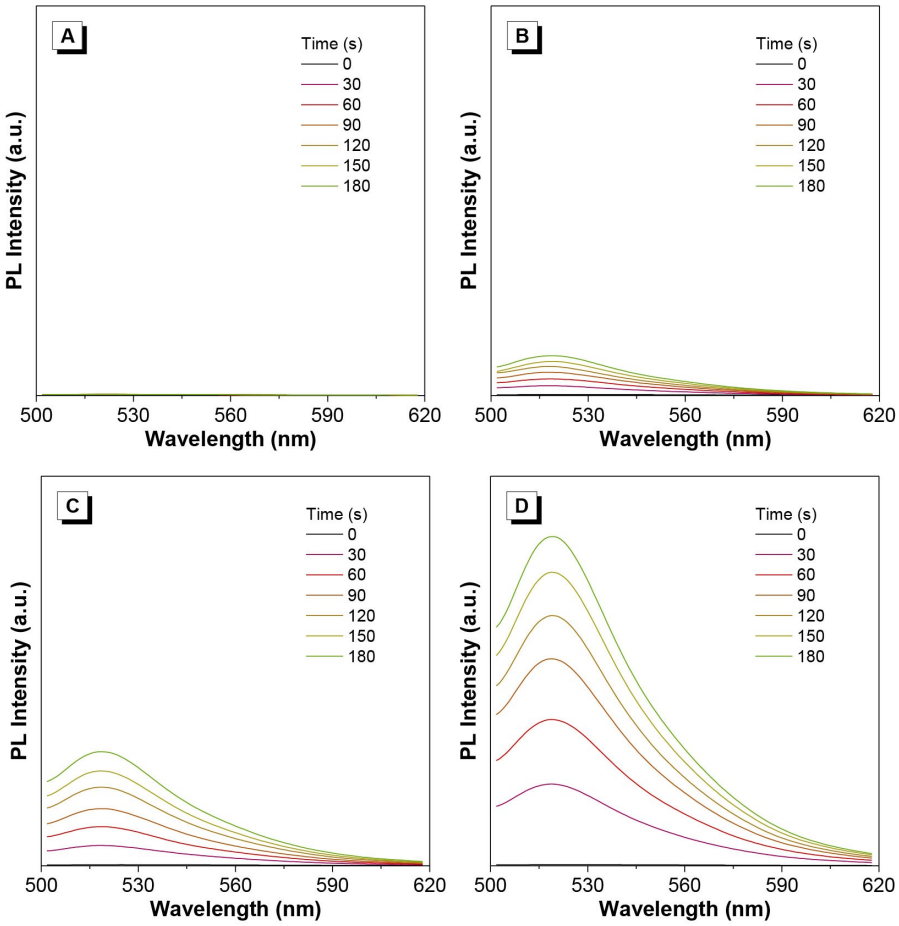

Fig. S15. PL spectra of HPF in the presence of (A) PBS, (B) **PPI-C0**, (C) **PPI-C1**, and (D) **PPI-C2** under white-light (400-700 nm, 100 mW cm^{-2}) irradiation. Concentration: complexes (2 μM), HPF (5 μM).

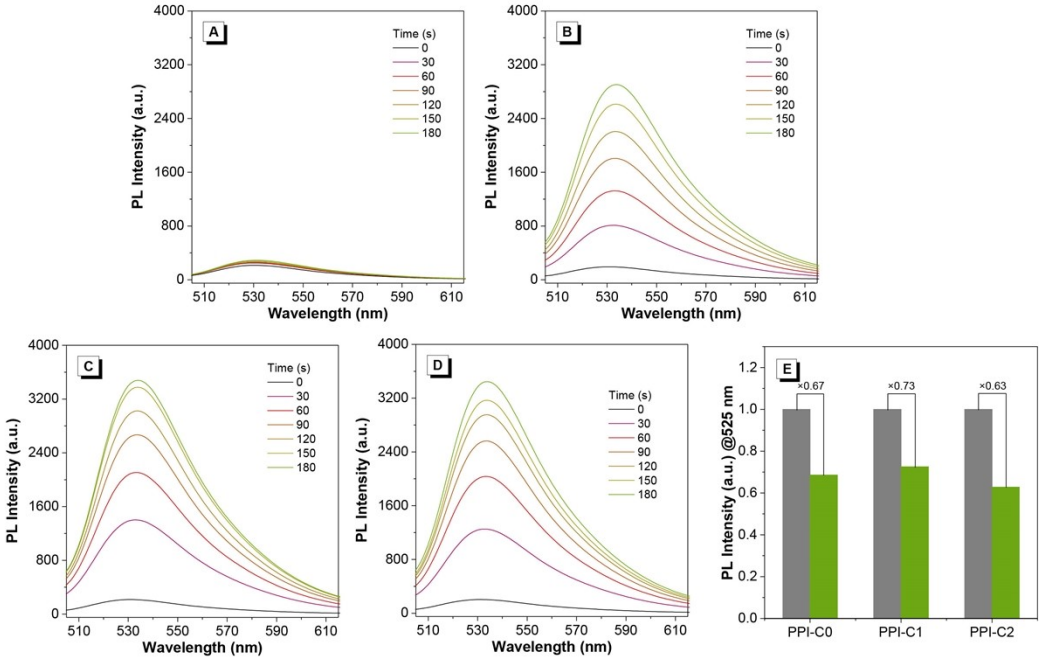

Fig. S16. PL spectra of DHR123 in the presence of (A) PBS, (B) **PPI-C0**, (C) **PPI-C1**, and (D) **PPI-C2** under white-light (400-700 nm, 100 mW cm^{-2}) irradiation. (E) Normalized PL intensity of DHR123 in the presence of **PPI-C0**, **PPI-C1** and **PPI-C2** with or without Vc under white-light (400-700 nm, 100 mW cm^{-2}) irradiation. Concentration: complexes (2 μM), DHR123 (5 μM).

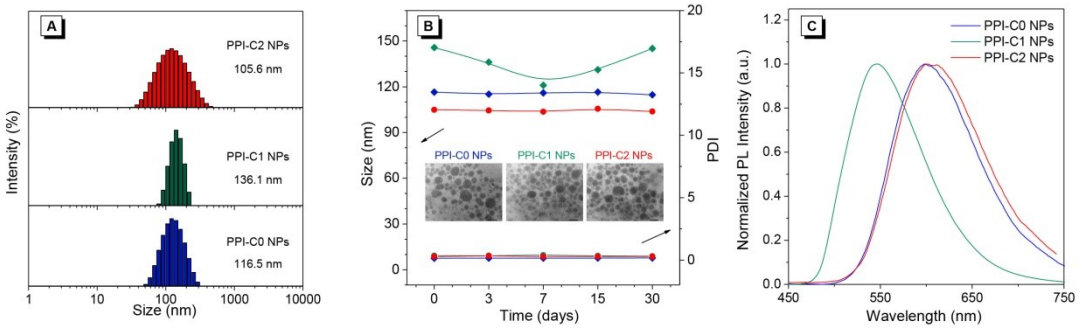

Fig. S17. (A) Size distribution of **PPI-C0** NPs, **PPI-C1** NPs, and **PPI-C2** NPs; (B) Stability and PDI changes of **PPI-C0** NPs, **PPI-C1** NPs, and **PPI-C2** NPs during 30 days, inset: TEM images of NPs. Scale bar = 200 μm. (C) PL intensity of **PPI-C0** NPs, **PPI-C1** NPs, and **PPI-C2** NPs in aqueous solution.

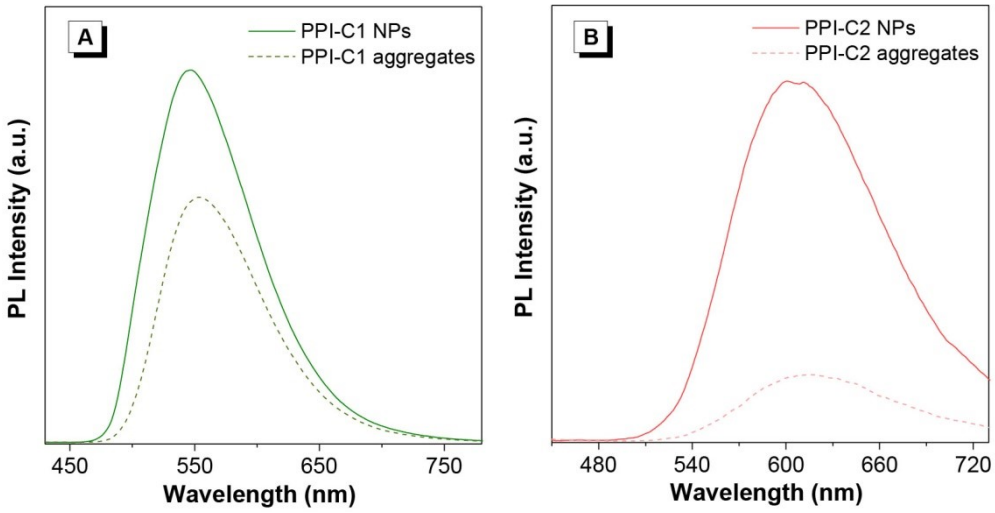

Fig. S18. Comparison of PL intensity in nanoparticle and aggregate states of (A) **PPI-C1** and (B) **PPI-C2** with same concentration. Concentration: 100 μg/mL.

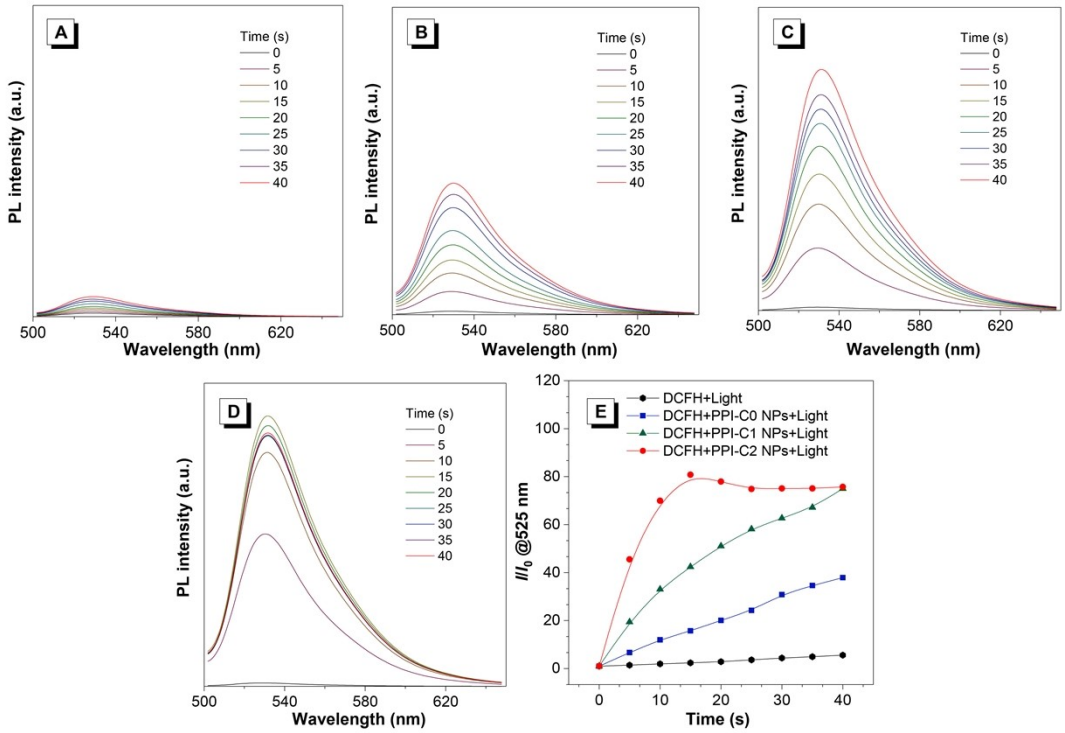

Fig. S19. PL spectra of DCFH-DA in the presence of (A) PBS, (B) **PPI-C0** NPs, (C) **PPI-C1** NPs, and (D) **PPI-C2** NPs. (E) Time-course plot of DCFH PL intensity enhancement in the presence of **PPI-C0**, **PPI-C1** and **PPI-C2**, respectively, under white-light (400-700 nm, 100 mW cm^{-2}) irradiation. Concentration: NPs (20 μg/mL), DCFH-DA (5 μM).

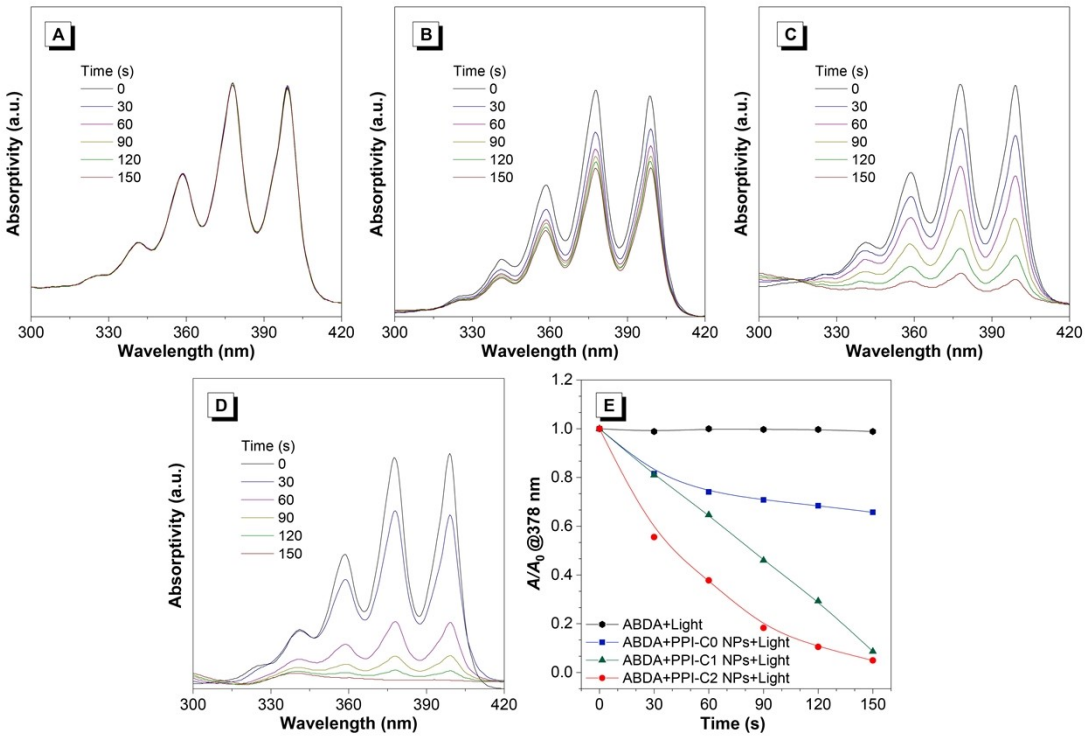

Fig. S20. Absorption spectra of ABDA in the presence of (A) PBS, (B) **PPI-C0** NPs, (C) **PPI-C1** NPs, and (D) **PPI-C2** NPs. (E) Time-course plot of ABDA decomposition in the presence of **PPI-C0**, **PPI-C1** and **PPI-C2**, respectively, under white-light (400-700 nm, 100 mW cm^{-2}) irradiation. Concentration: NPs (20 μg/mL), ABDA (20 μM).

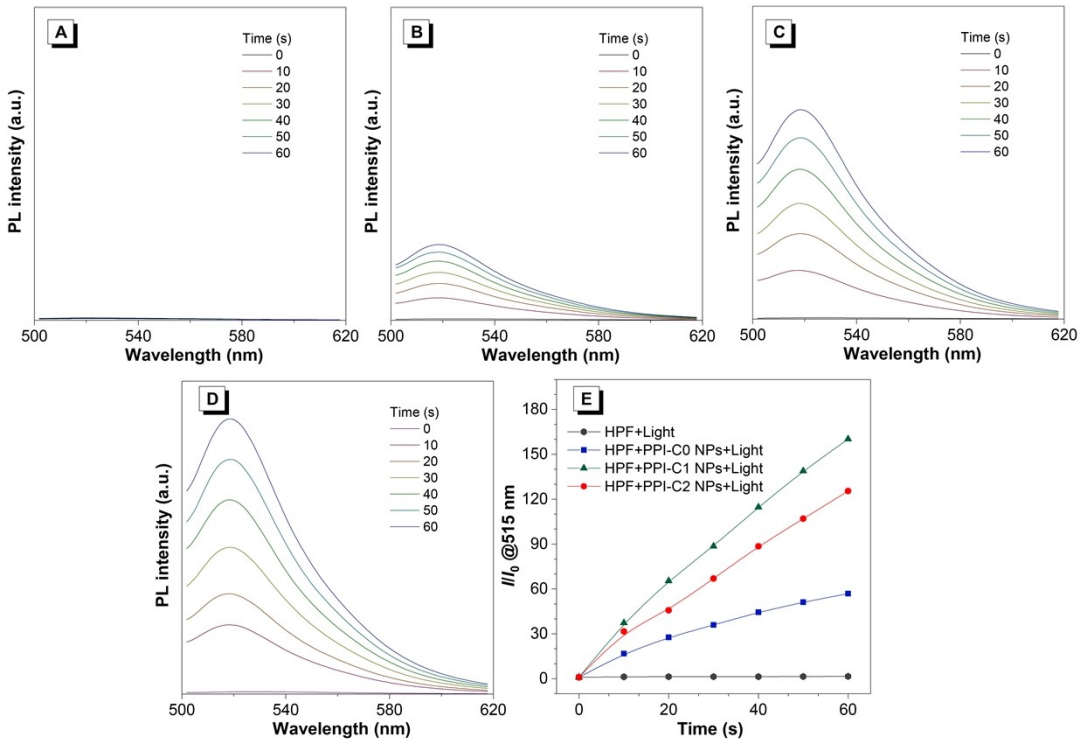

Fig. S21 PL spectra of HPF in the presence of (A) PBS, (B) **PPI-C0** NPs, (C) **PPI-C1** NPs, and (D) **PPI-C2** NPs. (E) Time-course plot of HPF PL intensity enhancement in the presence of **PPI-C0**, **PPI-C1** and **PPI-C2**, respectively, under white-light (400-700 nm, 100 mW cm^{-2}) irradiation. Concentration: NPs (20 μg/mL), HPF (5 μM).

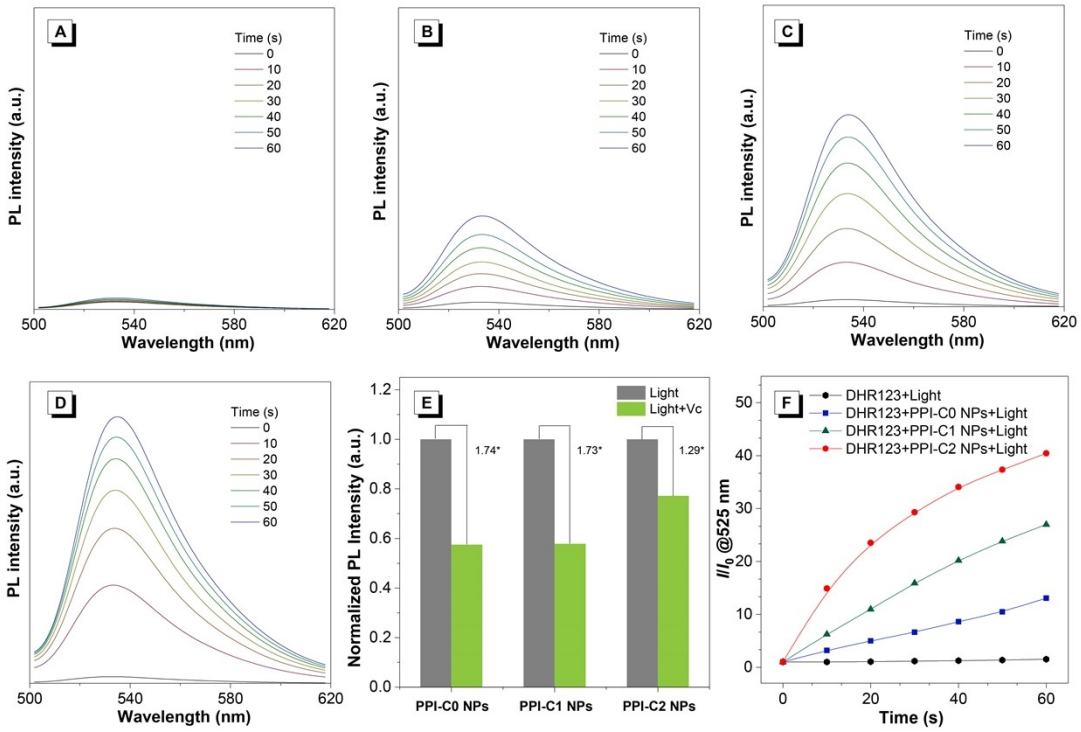

Fig. S22. PL spectra of DHR123 in the presence of (A) PBS, (B) **PPI-C0** NPs, (C) **PPI-C1** NPs, and (D) **PPI-C2** NPs. (E) Normalized PL intensity of DHR123 in the presence of **PPI-C0**, **PPI-C1** and **PPI-C2** NPs with or without Vc. (F) Time-course plot of DHR123 PL intensity enhancement of in the presence of **PPI-C0**, **PPI-C1** and **PPI-C2**, respectively, under white-light (400-700 nm, 100 mW cm^{-2}) irradiation. Concentration: NPs (20 μg/mL), DHR123 (5 μM).

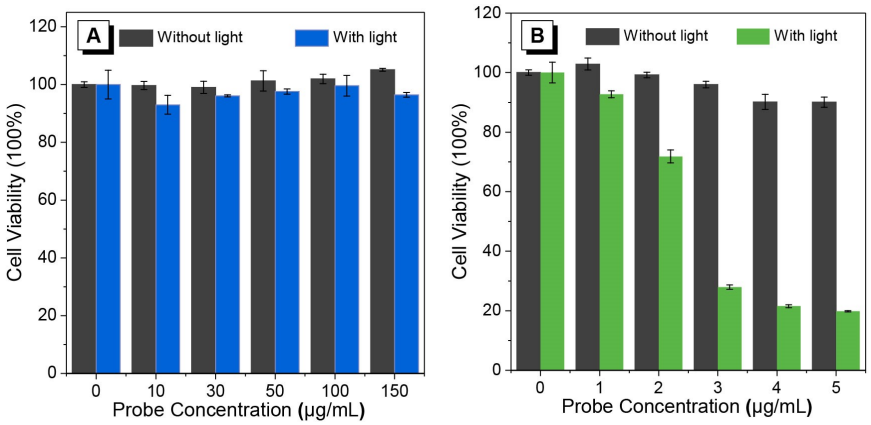

Fig. S23. Viability of Hela cells incubated with (A) **PPI-C0** and (B) **PPI-C1** NPs at different concentrations upon white-light (400-700 nm, 100 mW cm^{-2}) irradiation for 15 min.

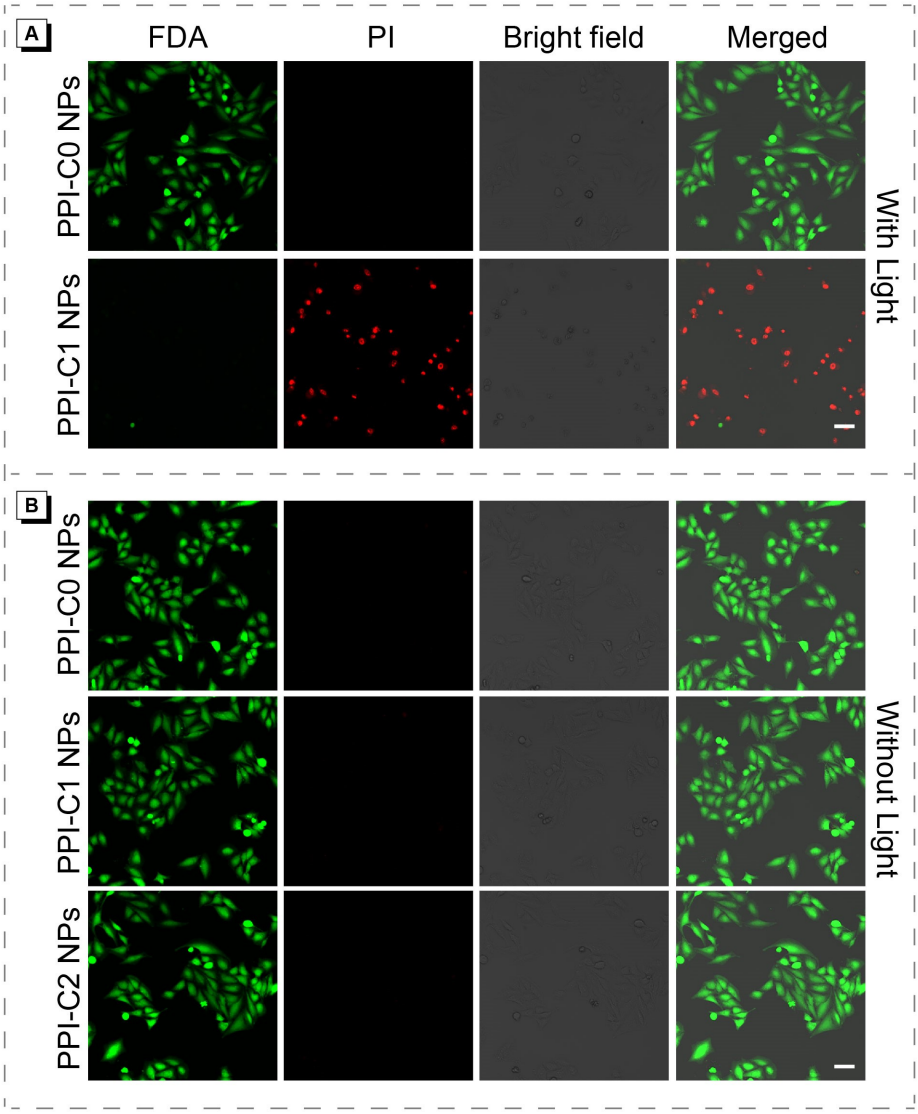

Fig. S24. Live/dead cell staining assays using FDA and PI as indicators treated with **PPI-C0** or **PPI-C1** NPs upon white light (400-700 nm, 100 mW cm^{-2}) irradiation for 15 min. Scale bar = 40 μm.

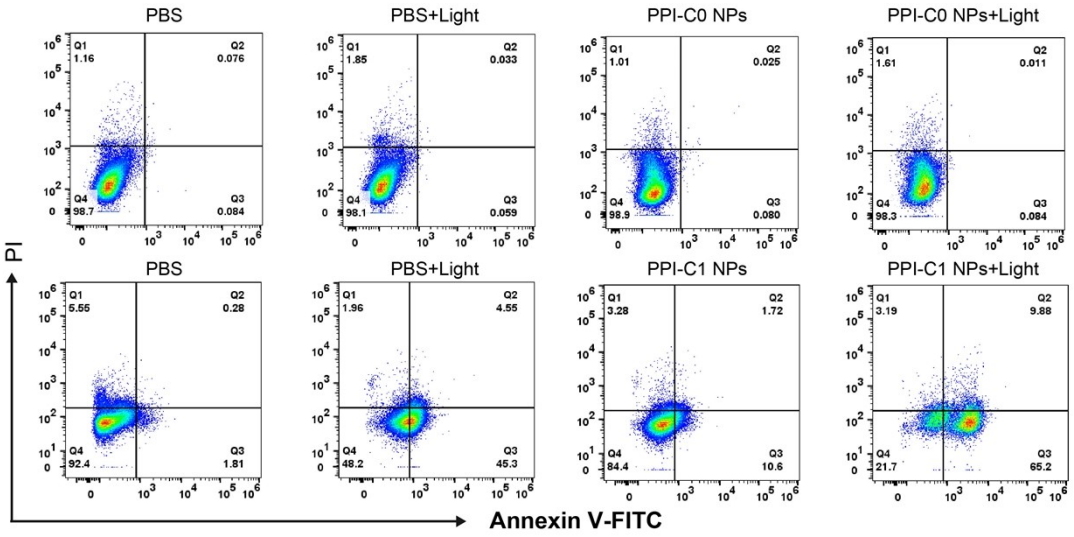

Fig. S25. Apoptosis analysis of Hela cells after different treatments with various formulations by FACS.

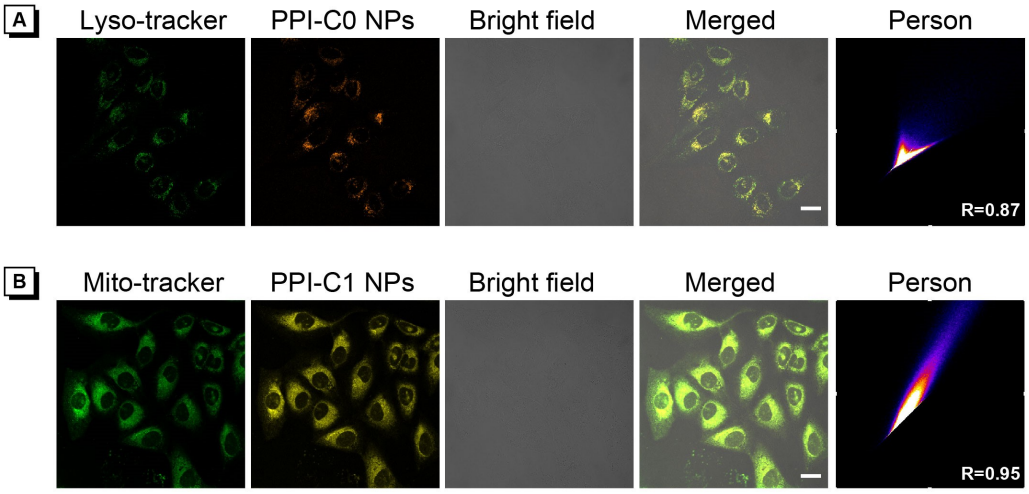

Fig. S26. CLSM images of HeLa cells incubated with (A) **PPI-C0** or (B) **PPI-C1** NPs for 8 h, followed by costaining with Lyso-tracker green or Mito-tracker green for 5 or 30 min. Scale bar = 20 μm. Concentration: NPs (10 μg/mL), Lyso-tracker green (25 nM), Mito-tracker green (100 nM).

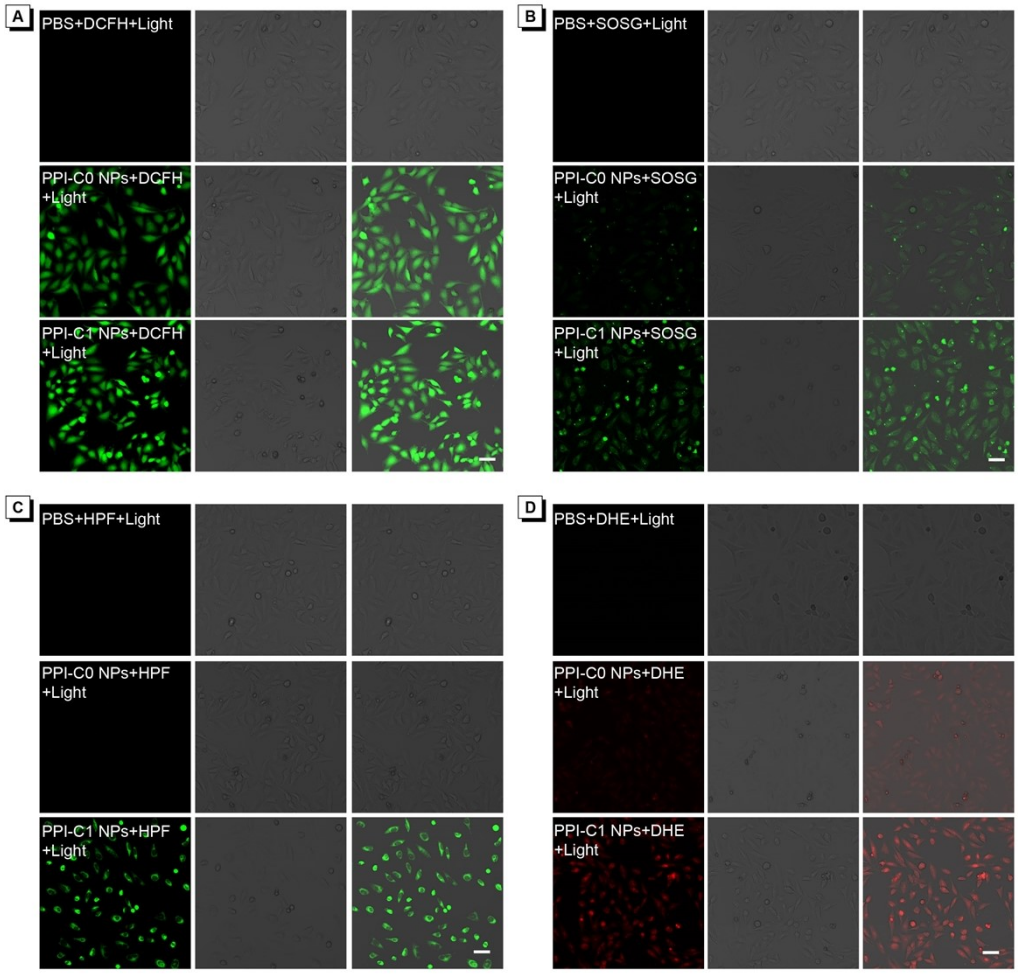

Fig. S27. Intracellular ROS generation by **PPI-C0** NPs and **PPI-C1** NPs with white light (400-700 nm, 100 mW cm^{-2}) irradiation inside Hela cells: (A) DCFH-DA for total ROS, (B) SOSG for $^1O_2$, (C) HPF for •OH, and (D) DHE for $•O_2^-$. Scale bar = 40 μm. Concentration: DCFH (10 μM), SOSG (10 μM), DHE (10 μM), HPF (10 μM).

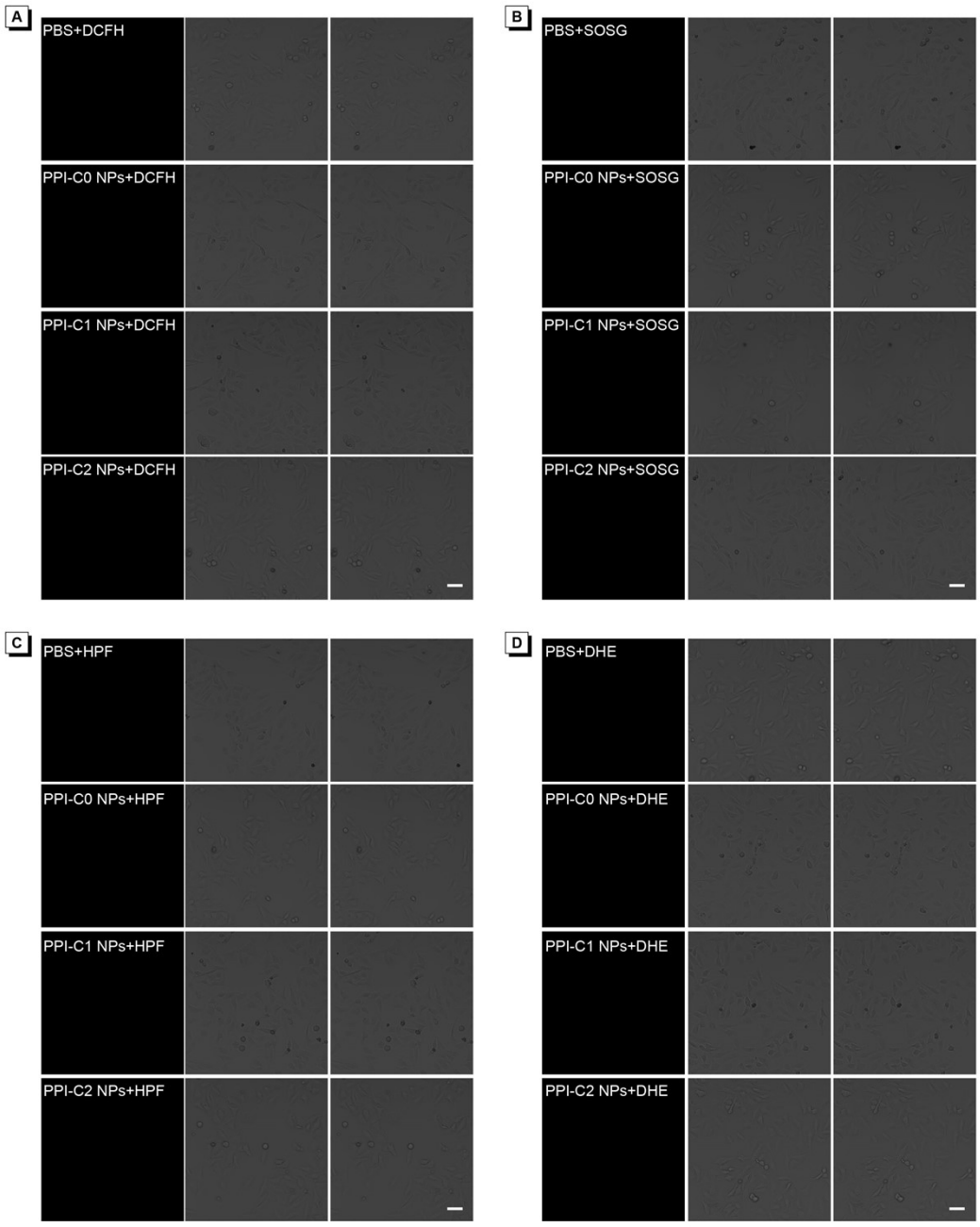

Fig. S28. Intracellular ROS generation by **PPI-C0** NPs, **PPI-C1** NPs and **PPI-C2** NPs without irradiation inside Hela cells: (A) DCFH-DA for total ROS, (B) SOSG for $^1O_2$, (C) HPF for •OH, and (D) DHE for $•O_2^-$. Scale bar = 40 μm. Concentration: DCFH (10 μM), SOSG (10 μM), DHE (10 μM), HPF (10 μM).

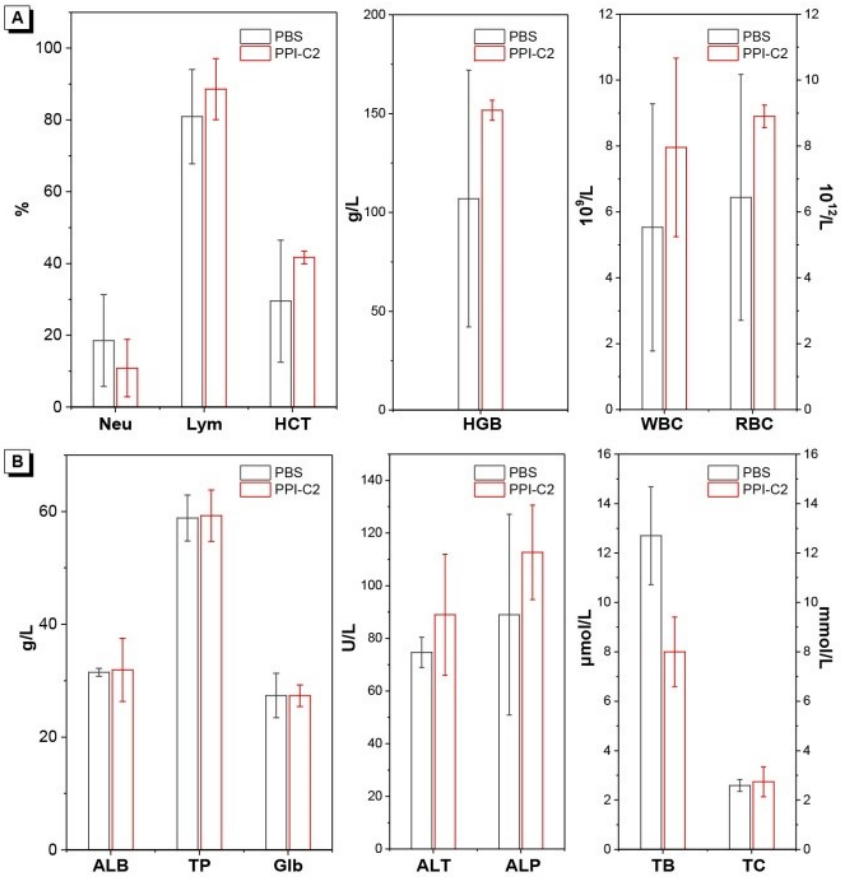

Fig. S29. Blood test results for treated BALB/c mice.

Table S1. Calculated excitation energies of the lowest triplet states (T_1) of **PPI-C0, PPI-C1 and PPI-C2**, dominant orbital excitations and oscillator strength.

	T_1	f	Assignment	Character
PPI-C0	2.10	0.00	HOMO→LUMO (88%)	^{3}MLCT/^{3}LLCT
PPI-C1	2.25	0.00	HOMO→LUMO (77%)	^{3}MLCT/^{3}LLCT
PPI-C2	2.10	0.00	HOMO→LUMO (91%)	^{3}MLCT/^{3}LLCT/ ^{3}ILCT

*H and L denote HOMO and LUMO, respectively.